Mathematical Modeling of Catalytic Converter Lightoff: Single-Pellet Studies

A detailed mathematical model of a single catalyst pellet has been developed to describe its behavior under transient conditions encountered during the warmup period of automobile exhaust catalytic converters. In contrast to the converter models previously reported in the literature, this model is capable of describing the time-dependent behavior of a composite catalyst pellet, and thus provides a convenient means of examining the effects of poison penetration and various noble metal impregnation strategies in the activity-time (rather than activity-temperature) domain.

Extensive calculations were carried out to investigate the effects of various catalyst design parameters and converter operating conditions on the lightoff behavior of a spherical, platinum-alumina catalyst pellet. Due to the complex kinetics of the CO and hydrocarbon oxidation reactions, catalyst lightoff was found to exhibit interesting behavior with respect to variations of the system's design parameters and operating conditions. Graphs are presented to illustrate the parametric sensitivity of these effects.

SE H. OH

JAMES C. CAVENDISH

and

L. LOUIS HEGEDUS

General Motors Research Laboratories
Warren, Michigan 48090

SCOPE

It has been widely recognized that a substantial fraction of the carbon monoxide and hydrocarbon emissions occurs during the first few minutes (i.e., warmup period) of the Federal Test Procedure (FTP) driving cycle. Therefore, it is crucial to improve converter warmup performance in order to meet automotive emission standards which mandate more stringent emission control. Since converter performance is a complex function of operating conditions, converter geometries, and catalyst properties, an empirical approach to the problem can be very costly and time-consuming; thus, mathematical modeling promises to be helpful in the development of catalytic converters with improved warmup performance.

There are some important design parameters associated with catalyst pellets used in automobile catalytic converters. For example, the relative locations of noble metals (Summers and Hegedus, 1978, Hegedus et al., 1979) and their impregnation depths (Hegedus and Summers, 1977) have been shown to have a strong influence on the performance and durability characteristics of automotive catalysts. Converter models previously developed (e.g., Kuo et al., 1971; Ferguson and Finlayson, 1974), however, were not designed to study the effects of the parameters associated with the design of the catalyst pellet.

Recently, Becker and Wei (1976, 1977a) investigated the effects of the location of the active layer on the catalyst's activity for negative-order reaction systems, such as the oxidation of carbon monoxide over platinum. They used the isothermal effectiveness factor vs. Thiele modulus plot to compare the lightoff characteristics of catalysts with various impregnation patterns. Although this approach is useful in gaining insight into the change in catalysts' activity as temperature varies, it does not provide information about the time scale of catalyst lightoff. Such information is necessary for estimating time-integrated emissions. For this reason, we decided to explore the time-dependent behavior of a catalyst pellet during the converter warmup process.

In this work a detailed transient single-pellet model has been developed to describe the time-dependent behavior of a catalyst pellet which is composed of concentric shells of differing physical and chemical properties. Such multilayered configuration, though an idealization of reality, has been used successfully for the modeling of automotive catalysts (Hegedus and Cavendish, 1977; Hegedus et al., 1977; Oh et al., 1978), and, as we will see, provides a convenient means of examining the effects of poison penetration and various noble metal impregnation strategies. This single-pellet model was then used to investigate the effects of catalyst properties and converter operating conditions on the lightoff characteristics of a spherical, alumina-supported platinum catalyst pellet for the oxidation of CO and propylene.

CONCLUSIONS AND SIGNIFICANCE

Some of the important findings are summarized below:

1. Under typical converter operating conditions, the lightoff behavior of a fresh catalyst pellet can be improved either by subsurface impregnation of the noble metal or by increasing its impregnation depth. However, the activity in the later portions of the warmup process is inferior to that of a surface-impregnated catalyst pellet with a shallow Pt band. In actual catalyst design, therefore, the beneficial effects of placing Pt subsurface or increasing the width of the Pt-impregnated shell on lightoff activity should be carefully weighed against possible detrimental effects on the catalyst's activity in the later stages of the warmup.

2. The beneficial effect of subsurface impregnation on catalyst lightoff was found to diminish at low CO concentrations or at high exhaust gas temperatures.

3. The poison-resistance of a catalyst can be improved either by increasing the noble metal impregnation depth or by placing Pt subsurface. However, if the Pt bandwidth is too large or if its location is too far away from the pellet's external surface, the fresh activity may be unacceptably low. Thus, a tradeoff must be made between fresh activity and poison resistance in selecting the location and width of the Pt band.

4. Rapid catalyst lightoff is favored by low pellet density. Plots are shown to quantify this effect.

5. Early activity can be improved slightly by decreasing the effective diffusivity in the pellet, but the catalyst's activity in

0001-1541-80-3251-0922-$01.15.

the later stages of the warmup process may be significantly degraded.

6. Catalyst lightoff is delayed with increasing CO or C_3H_6 concentrations in the exhaust gas, whereas increasing the O_2 concentration improves both lightoff and steady-state activity. Again, plots are shown to quantify these effects.

7. Faster lightoff occurs when a catalyst pellet is exposed to a higher exhaust gas flow rate.

8. At the early portions of the converter warmup process, significant temperature gradients are established inside the catalyst pellet. However, the intrapellet temperature profile becomes reasonably flat by the time the catalyst reaches its reaction temperature; thus, the assumption of uniform pellet temperature can be safely invoked in the modeling of catalytic converter lightoff.

The extension of the single-pellet model to a full-converter model is underway, and the results will be reported later.

INTRODUCTION

Several attempts have been made to develop mathematical models for pellet-type catalytic converters. Kuo et al. (1971) developed a cell model for the oxidation of carbon monoxide and hydrocarbons over a copper chromite catalyst, and the model predictions were successfully compared with converter performance data during the FTP driving cycle. Harned (1972) used a one-dimensional plug flow model to investigate the effects of various converter design parameters and operating conditions on the steady-state and warmup performance of a catalytic converter. In his work, the oxidation of CO and propylene was considered, and the conversion of propylene was assumed to be the same as CO conversion. Bauerle and Nobe (1973) presented a model describing the transient operation of a dual-bed catalytic converter (NO-CO reaction over copper chromite in the first bed and CO-O_2 reaction over copper oxide in the second bed). Recently Ferguson and Finlayson (1974) developed a transient converter model for the reduction of nitric oxide with CO and H_2 by employing a mixing cell scheme. The problem of diffusion-reaction interactions inside the catalyst pellet was solved efficiently by means of the orthogonal collocation method.

It has been shown (Becker and Wei, 1977a, 1977b; Hegedus and Summers, 1977; Summers and Hegedus, 1978; Hegedus et al., 1979) that the performance and durability characteristics of automobile catalytic converters can be significantly influenced by such catalyst design parameters as the relative location of noble metals and their impregnation depths. The previous converter models mentioned above, however, were not designed to include such details about the catalyst pellets, and thus are not well suited for studying the effects of the parameters associated with catalyst design.

In an attempt to provide useful guidance in the design of better catalysts and catalytic converters, we set out to develop a converter warmup model which includes some of the important design parameters of the catalyst pellets. As a first step toward this goal, a detailed transient single-pellet model has been developed, and extensive calculations were carried out to investigate the effects of catalyst properties and converter operating conditions on the warmup characteristics of the catalyst pellet.

This paper, the first part of our converter modeling studies, reports the results of these calculations based on the single-pellet model. In the second part to be published later, the single-pellet model will be extended to a full-converter model using a mixing cell scheme (Kuo et al., 1971; Ferguson and Finlayson, 1974), and the results of computations for converter warmup performance will be discussed. The present results are worth disclosing because, as the results of the full-converter model will show, the single-pellet model provides useful insight into the behavior of catalytic converter systems and points ways toward possible improvements in converter performance.

This work considers the lightoff behavior of a spherical, alumina-supported Pt catalyst for the oxidation of CO and propylene. The catalyst pellet is visualized as a multilayered composite porous medium. This approximation permits one to examine the effects of poison penetration and various noble metal impregnation strategies (i.e., the location and width of the Pt band) simply by assigning appropriate physical and chemical properties to the individual layers.

DEVELOPMENT OF MATHEMATICAL MODEL

Our model considers the following two representative oxidation reactions over Pt:

$$CO + 1/2\ O_2 \rightarrow CO_2$$

$$C_3H_6 + 9/2\ O_2 \rightarrow 3CO_2 + 3H_2O$$

Here the oxidation of "slow-oxidizing hydrocarbons," such as methane, is not included because these species are expected to have little influence on the catalyst's lightoff behavior as a result of their low reactivity. The effects of including H_2 in the simulation will be discussed later. Also note that the consideration of only oxidation reactions does not limit the applicability of our model, since oxidizing, three-way, and dual-bed converters all may warm up in the oxidizing mode.

The specific reaction rate expressions (that is, rates per unit Pt surface area) for carbon monoxide and propylene oxidation were obtained by calibrating the rate equations of Voltz et al. (1973) with our recycle reactor data. In this calibration, only the pre-exponential factors of the rate constants were adjusted, without changing the activation energies and adsorption equilibrium constants given by Voltz et al. The rate expressions used in our model are:

$$\tilde{R}_{CO} = \frac{k_{CO}c_{CO}c_{O_2}}{(1 + K_{CO}c_{CO} + K_{C_3H_6}c_{C_3H_6})^2} \quad \frac{\text{mol CO}}{\text{cm}^2\ \text{Pt} \cdot \text{s}} \tag{1}$$

$$\tilde{R}_{C_3H_6} = \frac{k_{C_3H_6}c_{C_3H_6}c_{O_2}}{(1 + K_{CO}c_{CO} + K_{C_3H_6}c_{C_3H_6})^2} \quad \frac{\text{mol } C_3H_6}{\text{cm}^2\ \text{Pt} \cdot \text{s}} \tag{2}$$

where

$$\left.\begin{aligned} k_{CO} &= 6.802 \times 10^{16} \exp(-13108/T) \\ k_{C_3H_6} &= 1.416 \times 10^{18} \exp(-15109/T) \\ K_{CO} &= 8.099 \times 10^{6} \exp(409/T) \\ K_{C_3H_6} &= 2.579 \times 10^{8} \exp(-191/T) \end{aligned}\right\} \tag{3}$$

From the stoichiometry, the reaction rate for oxygen is given by:

$$\tilde{R}_{O_2} = 1/2\ \tilde{R}_{CO} + 9/2\ \tilde{R}_{C_3H_6} \quad \frac{\text{mol } O_2}{\text{cm}^2\ \text{Pt} \cdot \text{s}} \tag{4}$$

It may be worth mentioning that although the pre-exponential factors of the kinetic parameters in Eqs. 1 and 2 become linearly dependent on T upon conversion of concentration units (from mol fraction used by Voltz et al. to mol/cm^3), the temperature dependence of the rate constants and adsorption equilibrium constants was found to be well approximated by the simple Arrhenius expressions with the constant pre-exponential factors given in Eq. 3.

Although only Pt catalysts are considered here, the essential features of our calculations are expected to carry over to other noble metals which exhibit negative-order kinetics.

Basic Equations

The conservation of reactive species i in a spherical catalyst pellet is described by:

$$\epsilon_p(r)\frac{\partial c_i}{\partial t} = \frac{1}{r^2}\frac{\partial}{\partial r}\left[D_{e,i}(r)r^2\frac{\partial c_i}{\partial r}\right] - a(r)\tilde{R}_i(\bar{c}, T) \tag{5}$$

$$i = 1(\mathrm{CO}),\ 2(\mathrm{C_3H_6}),\ 3(\mathrm{O_2})$$

where $\bar{c}$ is the vector whose elements are species concentrations c_1, c_2, and c_3. The boundary conditions are:

$$\frac{\partial c_i}{\partial r}(0, t) = 0 \tag{6}$$

$$\frac{\partial c_i}{\partial r}(R, t) = \frac{k_{m,i}}{D_{e,i}(R)}[c_{\infty,i}(t) - c_i(R, t)] \tag{7}$$

The radial dependence of the catalyst properties is explicitly shown in Eq. 5 to stress the fact that each layer of the catalyst pellet is permitted to have differing physical and chemical properties. In addition, we impose the continuity of both the concentration and the flux of the reacting species at the zone interfaces ($r = r_j$) for all $t \geq 0$:

$$c_i(r_{j-}, t) = c_i(r_{j+}, t) \tag{8}$$

$$D_{e,i}(r_{j-})\frac{\partial c_i}{\partial r}(r_{j-}, t) = D_{e,i}(r_{j+})\frac{\partial c_i}{\partial r}(r_{j+}, t) \tag{9}$$

The energy balance equation on the catalyst pellet is:

$$\rho_p(r)C_{ps}(r)\frac{\partial T}{\partial t} = \frac{1}{r^2}\frac{\partial}{\partial r}\left[\lambda_e(r)r^2\frac{\partial T}{\partial r}\right] + a(r)\sum_{i=1}^{2}\tilde{R}_i(\bar{c}, T)(-\Delta H)_i \tag{10}$$

with the boundary conditions:

$$\frac{\partial T}{\partial r}(0, t) = 0 \tag{11}$$

$$\frac{\partial T}{\partial r}(R, t) = \frac{h}{\lambda_e(R)}[T_\infty(t) - T(R, t)] \tag{12}$$

and the initial condition,

$$T(r, 0) = T^0(r) \tag{13}$$

Also, continuity conditions for T similar to Eqs. 8 and 9 are imposed at the zone interfaces.

In Eqs. 7 and 12, $c_{\infty,i}$ and T_∞ represent the concentration and temperature of the bulk gas phase surrounding the catalyst pellet, respectively. When the operation is carried out in a differential mode (e.g., a single catalyst pellet suspended in an infinite reservoir of gas), these values can be taken to be the same as the concentration and temperature of the incoming gas stream. However, the pellets in automotive catalytic converters typically operate in an integral mode, and their behavior has been shown to be well approximated by a mixing cell scheme (Kuo et al., 1971). In the mixing cell scheme, all the catalyst pellets in one cell are assumed to be exposed to a uniform (but different from the incoming stream) bulk gas phase condition. In the light of this observation, we were interested in investigating the behavior of the individual catalyst pellets in the mixing cell environment (rather than that of an isolated single catalyst pellet).

For a mixing cell of size V_{cell}, the boundary conditions at the pellet external surface (Eqs. 7 and 12) can be recast into the following more convenient form:

$$\frac{\partial c_i}{\partial r}(R, t) = \frac{k_{m,i}}{D_{e,i}(R)(1 + \alpha_i)}[c_{\mathrm{in},i}(t) - c_i(R, t)] \tag{14}$$

$$\frac{\partial T}{\partial r}(R, t) = \frac{h}{\lambda_e(R)(1 + \beta)}[T_{\mathrm{in}}(t) - T(R, t)] \tag{15}$$

where

$$\alpha_i = \frac{3k_{m,i}(1 - \epsilon)V_{\mathrm{cell}}}{QR} \tag{16}$$

$$\beta = \frac{3h(1 - \epsilon)V_{\mathrm{cell}}}{QR\rho_g C_{pg}} \tag{17}$$

The detailed derivation of Eqs. 14 and 15 can be found elsewhere (Ferguson and Finlayson, 1974). This rearrangement allows us to express the boundary conditions in terms of known inlet gas conditions, $c_{\mathrm{in},i}$ and T_{in}.

This study simulates the transient response of a catalyst pellet, initially at room temperature, following a step flow of stabilized exhaust gas at an elevated temperature. Although surface phenomena (i.e., adsorption, desorption, and surface reaction) have been shown to be important in determining the transient response of supported catalysts under isothermal conditions (Oh et al., 1978), such processes are not included in our model since the thermal response of the pellet is expected to dominate the dynamic behavior of the whole system.

Note that for our calculations the accumulation of mass in the catalyst pellet was neglected (i.e., $\partial c_i/\partial t = 0$ in Eq. 5; quasistatic approximation), since its time constant is typically much smaller than that of the pellet thermal response (Kuo et al., 1971; Ferguson and Finlayson, 1974) and consequently the intrapellet concentration profiles would quickly approach an asymptotic equilibrium with respect to the pellet temperature. We also assume that the physical and chemical properties of the catalyst pellet are piecewise constant; that is, they are constant within each layer of the pellet, but these constants are allowed to vary from layer to layer.

Once the quasistatic approximation is invoked for the mass balance equations on the catalyst pellet, one would be tempted to use the steady-state effectiveness factor vs. Thiele modulus curve to obtain the reaction rates under the influences of intra- and interpellet diffusion resistances, as was done by Kuo et al. (1971) and by Harned (1972). This would greatly reduce the computation time. In our case, however, this approach cannot be used even in the presence of excess oxygen, because of the coupling between CO and $\mathrm{C_3H_6}$ in the kinetic expressions (Eqs. 1 and 2); that is, the effectiveness factor for the CO-$\mathrm{O_2}$ reaction depends on the extent of the $\mathrm{C_3H_6}$-$\mathrm{O_2}$ reaction and vice versa. Consequently, the single-pellet equations (two-point boundary value problem) must be solved repeatedly.

Parameter Evaluation

The effective diffusivities of CO, $\mathrm{C_3H_6}$, and $\mathrm{O_2}$ were calculated from the random pore model of Wakao and Smith (Smith, 1970) using the pore size distribution data of a typical automotive catalyst pellet. The effective diffusivities were assumed to increase with the 1.4th power of temperature. The molecular diffusivity of the reactants in the reaction mixture was approximated by estimating the bimolecular diffusivity of the species in $\mathrm{N_2}$ using the Slattery-Bird formula (Bird et al., 1960). The correlation of De Acetis and Thodos (1960) was used to calculate the external heat and mass transfer coefficients.

The size of a mixing cell is generally a function of the degree of axial dispersion in the bed and converter geometry. In our calculations, the mixing cell volume was taken to be 1065 $\mathrm{cm^3}$, which amounts to approximating a type 260 production converter by four mixing cells. This choice of cell size seems reasonable in view of the analysis and experiment described by Wei (1975), which suggests three to four pellet layers for one mixing cell.

The local Pt surface area, $a(r)$, in Eqs. 5 and 10 can be calculated from known values of Pt wt % and dispersion as:

$$a = 2.6 \times 10^6\left(\frac{R^3}{r_1^3 - r_2^3}\right)\left(\frac{\text{disp. \%}}{100}\right)\left(\frac{\text{wt \%}}{100}\right)\rho_p, \quad \frac{\mathrm{cm^2\ Pt}}{\mathrm{cm^3\ pellet}}$$

where r_1 and r_2 represent the outer and inner boundaries of the impregnated zone, respectively.

Numerical Solution of the Equations

In the quasistatic model we seek numerical approximations to the coupled equations (Eqs. 5 and 10):

$$R_{e,i}[\bar{c},\ T,\ r] \equiv \frac{1}{r^2}\frac{d}{dr}\left[D_{e,i}(r)r^2\frac{dc_i}{dr}\right] - a(r)\tilde{R}_i(\bar{c},\ T) = 0 \quad (18)$$
$$(1 \le i \le 3,\ 0 < r < R)$$

$$R_{e,T}[\bar{c},\ T,\ r,\ t] \equiv \frac{1}{r^2}\frac{\partial}{\partial r}\left[\lambda_e(r)r^2\frac{\partial T}{\partial r}\right] + a(r)\sum_{i=1}^{2}\tilde{R}_i(\bar{c},\ T)(-\Delta H)_i - \rho_p(r)C_{ps}(r)\frac{\partial T}{\partial t} = 0 \quad (19)$$
$$(0 < t,\ 0 < r < R)$$

subject to the boundary conditions given by Eqs. 6, 11, 14, and 15; initial condition for T by Eq. 13; interface conditions for c_i by Eqs. 8 and 9; and similar interface conditions for T. While Eq. 18 is a *steady-state* two-point boundary value problem, Eq. 19 is a *transient* two-point boundary value problem. In Eqs. 18 and 19, both physical [$D_{e,i}(r)$, $\lambda_e(r)$, $\rho_p(r)$, and $C_{ps}(r)$] and chemical [$a(r)$] properties are permitted to vary discontinuously from region to region in the catalyst pellet. Galerkin's method with piecewise analytic trial functions has proven to be an effective technique for solving such composite material problems (Hegedus and Cavendish, 1977; Oh et al., 1978).

Galerkin's method is one of several methods of weighted residuals (Finlayson, 1972). In the Galerkin formulation, the unknown solution (c_i and T) is first represented as a sum of known basis functions $w_j(r)$ with arbitrary expansion coefficients $a_i^j(t)$ and $b^j(t)$:

$$c_i(r,\ t) \cong \hat{c}_i(r,\ t) = \sum_{j=1}^{M} a_i^j(t)\ w_j(r) \quad (1 \le i \le 3) \quad (20)$$

$$T(r,\ t) \cong \hat{T}(r,\ t) = \sum_{j=1}^{M} b^j(t)\ w_j(r) \quad (21)$$

Here $\hat{c}_i(r,\ t)$ and $\hat{T}(r,\ t)$ are the Galerkin approximations to the solution of the problem, and the time-dependent expansion coefficients $a_i^j(t)$ and $b^j(t)$ are to be determined such that $\hat{c}_i(r,\ t)$ and $\hat{T}(r,\ t)$ given by Eqs. 20 and 21 are accurate approximations to $c_i(r,\ t)$ and $T(r,\ t)$ for all $0 \le r \le R$, $0 \le t$. If $\hat{c} \equiv (\hat{c}_1, \hat{c}_2, \hat{c}_3)$, the expansion coefficients are determined by the conditions that the residuals given by Eqs. 18 and 19 be orthogonal to the basis function $w_j(r)$ for $j = 1,2, \ldots, M$:

$$\left.\begin{aligned}\int_0^R R_{e,i}[\hat{c},\ \hat{T},\ r]w_j(r)r^2dr = 0 \\ \int_0^R R_{e,T}[\hat{c},\ \hat{T},\ r,\ t]w_j(r)r^2dr = 0\end{aligned}\right\} \begin{aligned}1 \le i \le 3 \\ 1 \le j \le M\end{aligned} \quad (22)$$

In the Appendix we develop the Galerkin's method in detail, focusing on practical questions regarding the choice of basis functions, numerical evaluation of integrals arising from the method, and the techniques used to integrate the coupled transient and steady-state equations.

RESULTS AND DISCUSSION

Table 1 shows a standard set of parameter values used for the calculations. We will perturb these parameters separately and in combination to investigate the lightoff behavior of a catalyst pellet as a function of converter operating conditions and catalyst design parameters. The exhaust gas composition and flow rate listed in Table 1 are similar to the test conditions of an engine dynamometer system developed for the evaluation of converter lightoff (Herod et al., 1973); however, a somewhat lower exhaust temperature was chosen here so that differences in the lightoff behavior of various catalysts would be more pronounced and thus easier to observe. This aspect will become more apparent later. Also, the catalyst pellet is assumed to be

TABLE 1. STANDARD SET OF PARAMETER VALUES

Catalyst Pellet

0.05 wt % Pt (80% dispersion when fresh)
ρ_p = 1.0 g/cm^3
R = 0.1750 cm
$D_{e,CO}$ = 0.0487 cm^2/s
D_{e,C_3H_6} = 0.0360 cm^2/s } at 838 K, 101.3 kPa
D_{e,O_2} = 0.0469 cm^2/s
C_{ps} = 0.8374 J/g · K
λ_e = 1.8 × 10^{-3} J/cm · s · K
T^o = 300 K

Converter

Volume = 4261 cm^3 (Type 260)
Frontal Area = 838.7 cm^2 (=130 in.^{2})
ϵ = 0.4

Exhaust Gas

$c_{in,i}$ = { 2 vol % CO; 0.05 vol % C_3H_6 (=500 ppm); 3 vol % O_2 }
T_{in} = 550 K
Q = 33 000 cm^3/s (at 295 K, 101.3 kPa)
P = 101.3 kPa
C_{pg} = 1.046 J/g · K

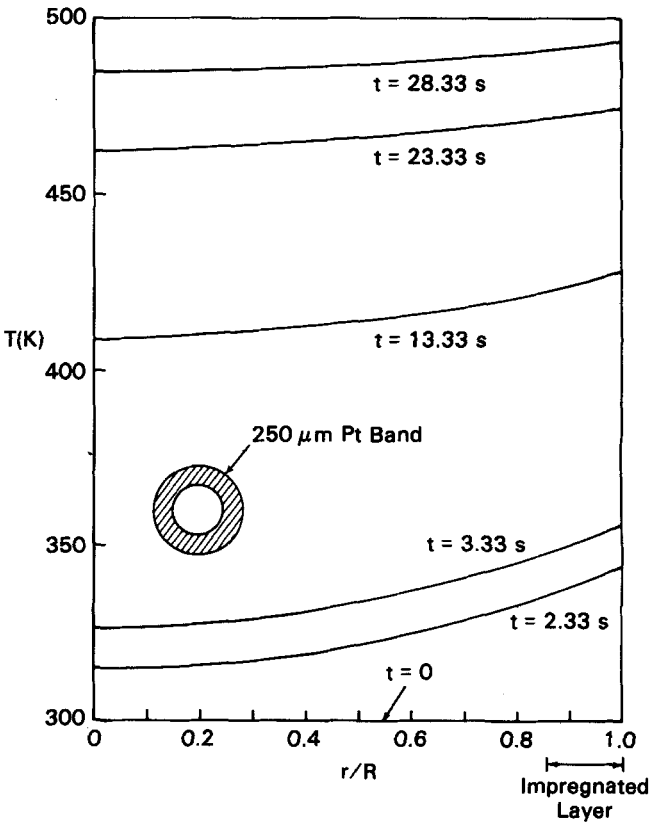

Figure 1. Time variation of intrapellet temperature profile; parameter values are listed in Table 1.

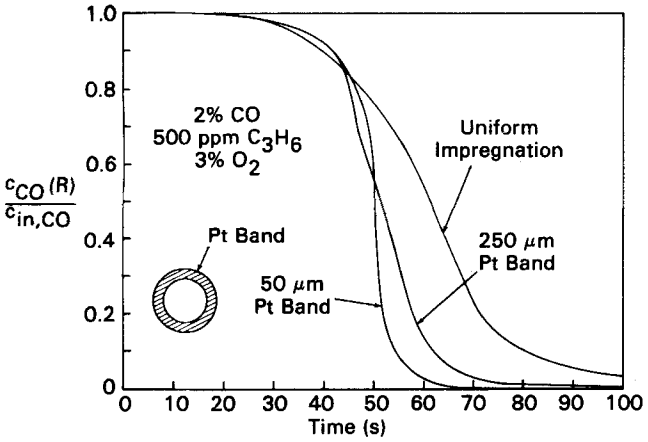

Figure 2. Effects of impregnation depth for surface-impregnated catalysts at the standard conditions listed in Table 1.

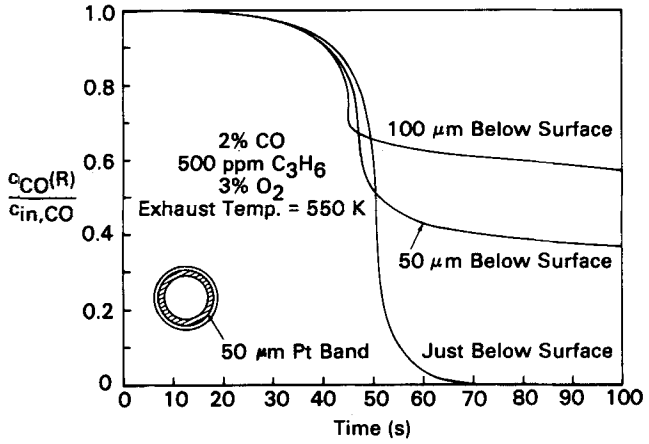

Figure 3. Effects of the location of Pt band (50 μm thick) at the standard conditions listed in Table 1.

initially at room temperature (i.e., T^o = 300K) in view of the FTP test procedure.

Before discussing the results of our parametric study, it may be instructive to observe the typical concentration and temperature profiles in the catalyst pellet as a function of time, after a cold pellet has been subjected to a step flow of hot exhaust gas at $t = 0$. Figure 1 shows the time variation of the intrapellet temperature profile for a surface-impregnated catalyst (250 μm thick Pt band). Other parameter values were taken to be the same as those listed in Table 1. Figure 1 shows that at early times, significant temperature gradients (about 30 K for $t < 3$ s) are established in the catalyst pellet. However, due to heat conduction inside the pellet, the temperature gradient tends to diminish with increasing time, and consequently by the time the pellet is heated up to the reaction temperature (say, $t > 30$ s), the intrapellet temperature profile becomes relatively flat. This aspect has useful implications in simplifying the model, and will be discussed in more detail later.

The corresponding computed intrapellet concentration profiles show that the CO and C_3H_6 concentration levels in the inner (inert) core of the pellet decrease as the catalyst pellet is warming up, and their gradients near the pellet's outer edge become increasingly steep with increasing time. It is interesting to note that although the lightoff of C_3H_6 is slightly slower than that of CO, the time scales of lightoff for both species are predicted to be very similar, presumably due to their kinetic coupling effects. Because of this similarity between CO and C_3H_6 and since the concentration at the pellet's external surface is a direct measure of the reaction rate within a catalyst pellet (that is, the rate per one pellet is proportional to $[c_{in,i} - c_i(R)]$), we will use a plot of $c_{CO}(R)/c_{in,CO}$ vs. time in subsequent figures in order to illustrate the transient response of the catalyst pellet after a step change in the bulk gas phase condition.

Figure 2 compares the step responses of fresh, surface-impregnated catalysts. Here the Pt band is located near the pellet's external surface, and a fixed amount of Pt (0.05 wt %) is distributed over three different band widths. It can be seen that upon increasing the impregnation depth, some improvement in early activity is obtained, but the catalyst activity in the later portions of the warmup process is inferior to that of a catalyst with a shallow Pt band. It is of interest to note that at the steady state (e.g., $t > 100$ s) the effect of impregnation depth variation disappears and the catalysts' activity is limited by external mass transfer, due to the high pellet temperature attained as a result of the reaction exotherm.

Figure 3 shows the effects of the location of the Pt band on the transient behavior of fresh catalysts. Here both the Pt content (0.05 wt %) and the Pt band width (50 μm) are kept constant. The calculations show that placing Pt away from the pellet's outer edge benefits catalyst lightoff, but only at the expense of deteriorating steady-state activity, because of the diffusion resistances of the outer inert shell. In actual catalyst design, therefore, the possible beneficial effect of subsurface impregnation on catalyst lightoff must be balanced against its detrimental effect on the steady-state activity.

The improvement in early-time activity, predicted for the cases of subsurface impregnation (Figure 3) and a thick Pt band (Figure 2), is the result of the interaction between the negative-order kinetics and intrapellet diffusion resistances (Becker and Wei, 1976, 1977a). Accordingly, such improvement is expected to diminish when the catalyst's operating conditions are shifted away from the regime of negative-order kinetics. For example,

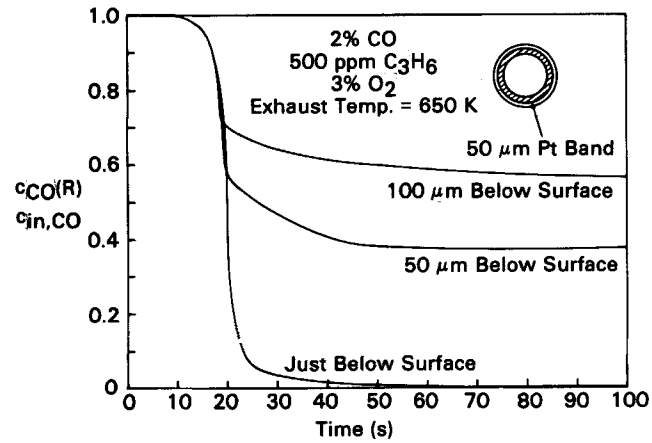

Figure 4. Effects of the location of Pt band (50 μm thick) at T_{in} = 650 K; other parameter values are listed in Table 1.

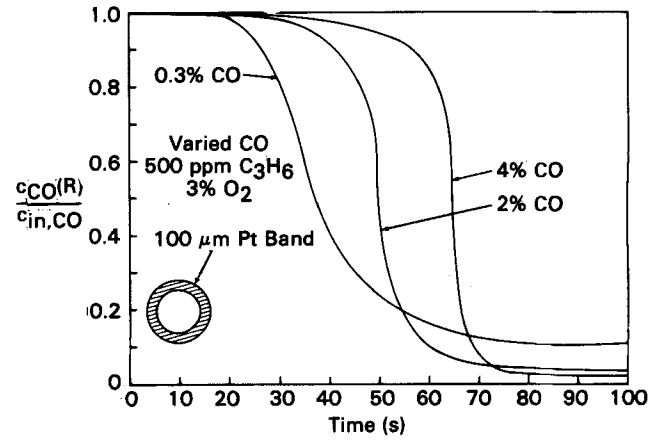

Figure 5. Effects of CO concentration in the exhaust; other parameter values are listed in Table 1.

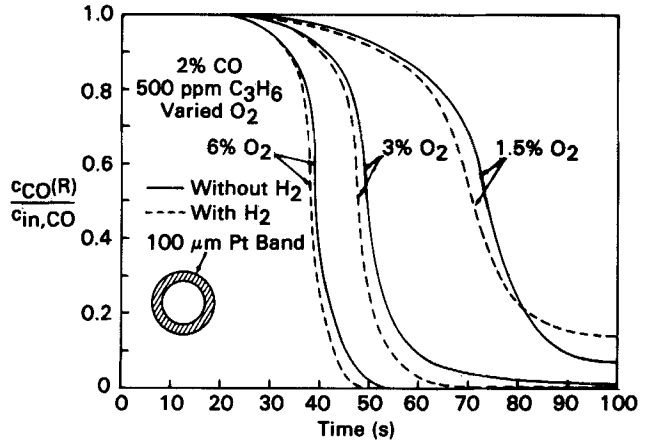

Figure 6. Predicted transient behavior with and without H_2 for various O_2 concentration levels; other parameter values are listed in Table 1.

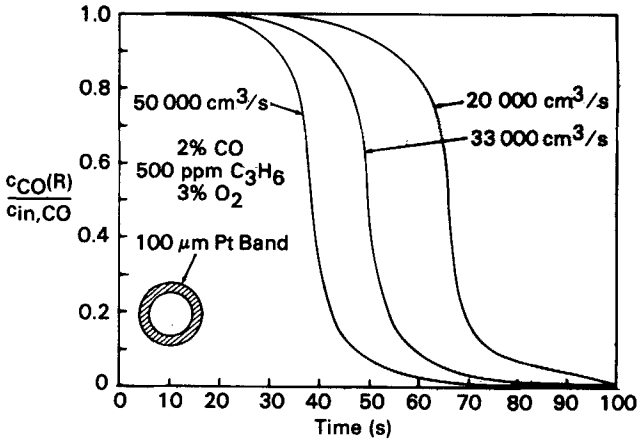

Figure 7. Effects of exhaust gas flow rate (flow rates shown here at 295 K, 101.3 kPa); other parameter values are listed in Table 1.

when the CO concentration in the exhaust is reduced to 0.3 vol%, the calculations show that the benefit of the subsurface impregnation disappears.

In actual converter operation, the converter inlet CO concentration is a function of the choke schedule of the particular vehicle system. A fast choke schedule, for example, may result in relatively low CO concentrations at the time of catalyst lightoff. On the other hand, catalytic converters which warm up quickly may face higher CO concentrations during catalyst lightoff. Therefore, the proper catalyst impregnation strategy depends, to a certain extent, on the choke schedule of the particular vehicle system under consideration.

The effect of the exhaust gas temperature is also interesting in this regard. Comparison of Figures 3 and 4 shows that increasing the exhaust temperature gives the expected benefit of earlier catalyst lightoff for all the impregnation patterns considered here. More interestingly, however, the advantage of placing the Pt band subsurface diminishes when the exhaust temperature is increased to 650 K (Figure 4), which represents a typical converter inlet temperature encountered during the converter warm-up process (Herod et al., 1973). The latter effect can be attributed to the fact that with increasing the exhaust temperature, the catalyst's lightoff behavior is increasingly dominated by the process of pellet warmup due to convective heat transfer between the exhaust gas and the pellets, and consequently becomes less sensitive to the noble metal impregnation patterns.

Figure 5 shows the effects of the CO concentration in the exhaust for a fresh, surface-impregnated catalyst (100 μm thick Pt band). The catalyst lightoff is delayed substantially (and becomes sharper) upon increasing the CO concentration, as can be anticipated from the negative-order kinetics of the CO oxidation. Notice, however, that after lightoff, the intrapellet CO concentration drops to a lower level with higher CO concentration, due to the associated stronger reaction exotherm. It should also be noted that variations in C_3H_6 concentration affect the catalyst's lightoff behavior in a similar fashion: the lightoff is delayed with increasing C_3H_6 concentrations.

The computational results for various O_2 concentrations (Figure 6) show that both lightoff and steady-state oxidation performance can be improved by increasing the O_2 concentration in the exhaust. Injecting additional air into the exhaust upstream of the converter using an air pump appears to be a convenient way of increasing the O_2 concentration; however, converter cooling effects arising from the additional cold air injected must be considered. It is worth mentioning that, as Figure 6 indicates, the catalyst's activity is particularly sensitive to the O_2 concentration variation in the presence of a near-stoichiometric amount of O_2 (compare 1.5% O_2 with 3% O_2); however, the benefit from a further increase in O_2 concentration is predicted to be small, even without considering the cooling effects mentioned above (compare 3% O_2 with 6% O_2).

Figure 6 also shows the comparison of predicted transient response with and without H_2 for three different O_2 concentration levels. The effect of H_2 is particularly interesting because of its heat of reaction and its demand for O_2. It has often been assumed that the concentration of H_2 is one-third of that of CO everywhere in the converter (Kuo et al., 1971; Young and Finlayson, 1976). The computational results based on this assumption (dotted lines) are shown in Figure 6, along with the results for the case of no H_2 (solid lines). It is of interest to see that including H_2 in the simulation does not significantly change the predictions of catalyst lightoff, over a wide range of O_2 concentrations considered here. This can be attributed to the fact that

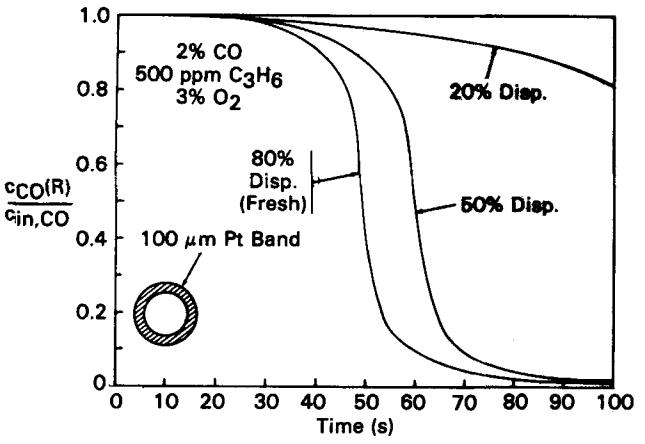

Figure 8. Effects of noble metal dispersion; other parameter values are listed in Table 1.

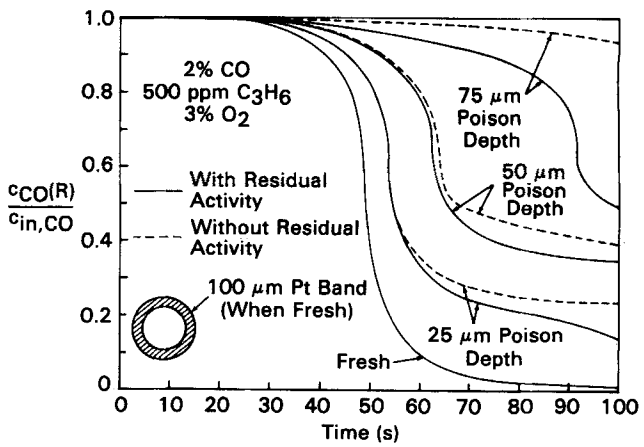

Figure 9. Effects of the depth of poison penetration with and without residual activity; other parameter values are listed in Table 1.

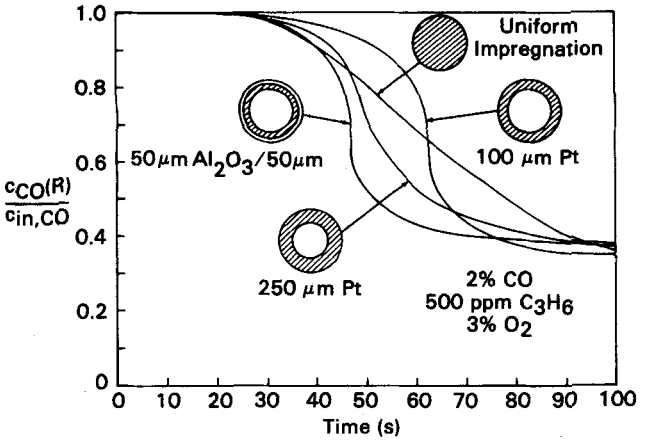

Figure 10. Lightoff behavior after 50 μm poison penetration for various impregnation strategies; other parameter values are listed in Table 1.

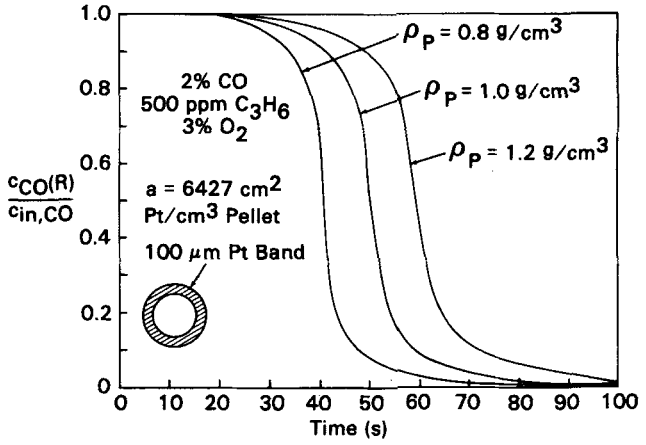

Figure 11. Effects of pellet density (and associated effective diffusivity) on the lightoff behavior of a catalyst; other parameter values are listed in Table 1.

the increased heat of reaction is counterbalanced, to a certain extent, by the decreased O_2 availability to oxidize CO.

Figure 7 shows the effect of exhaust gas flow rate. Catalyst lightoff is seen to be enhanced by high flow rates, largely due to the attendant increase in the gas-particle heat transfer coefficient and thus faster catalyst pellet warmup. Note, however, that this effect does not necessarily translate into a reduction in the emissions of CO and C_3H_6, because their amounts introduced into the converter per unit time are directly proportional to the exhaust flow rate.

It is well known that high-temperature exposure of the catalyst promotes the sintering of Pt which reduces the amount of the noble metal available for catalytic reactions (i.e., decreased dispersion). Figure 8 shows that both lightoff and steady-state performance deteriorate upon sintering. The reduction of the noble metal loading is expected to show a similar effect.

Another item of practical interest is the effect of catalyst poisoning. Under typical converter operating conditions, the poisonous species in the engine exhaust (e.g., *P*) penetrate the pellets in the form of a reasonably sharp front, without plugging the pores. As shown in Figure 9, the catalyst's activity is, of course, impaired by the poison penetration. In the calculations, the intrapellet effective diffusivities were assumed to remain unchanged upon poisoning, and one-twentieth of the fresh activity was assigned to the poisoned Pt layer for both CO and C_3H_6 oxidation (solid lines in Figure 9), in view of independent experiments with phosphorus-poisoned platinum catalysts (Hegedus and Summers, 1975; Schlatter, 1976). The computational results based on the assumption of zero residual activity in the poisoned shell are also included in Figure 9 (dotted lines) to allow a direct comparison. It can be seen that the contribution of the residual activity becomes more pronounced with increasing poison penetration depth; for the poison depth of 75 μm, for example, the model predicts considerably higher catalyst activity (especially at the steady state) when the residual activity is accounted for.

Figure 10 compares the transient response of a single catalyst pellet after 50 μm poison penetration for four different Pt impregnation patterns. Here again, it was assumed that one-twentieth of the original activity was retained in the poisoned layer. The results of Figure 10 indicate that the activity of partially poisoned catalysts can be improved either by placing Pt subsurface or by increasing the Pt impregnation depth (compare the cases of 100 μm Pt and 250 μm Pt). Notice, however, that if the impregnation depth is too large (the curve for uniform impregnation), the catalyst lightoff becomes sluggish, resulting in the deterioration of overall performance.

The poison resistance of supported catalysts can also, of course, be improved by reducing the rate of poison penetration. This can be achieved, for example, by a proper choice of the pore structure and support surface area, as discussed in a recent paper by Hegedus and Summers (1977).

The density of catalyst pellets is an important design parameter in developing a catalyst which warms up quickly. As shown in Figure 11, the lightoff characteristics of the catalyst are improved as the pellet density is decreased. Since a convenient way of varying pellet density is to modify the pore structure of the catalyst support, the associated change in the effective diffusivities was also incorporated in the calculations. (The effective diffusivities were calculated to increase by 8% when the pellet density was reduced from 1 to 0.8 g/cm^3, assuming that

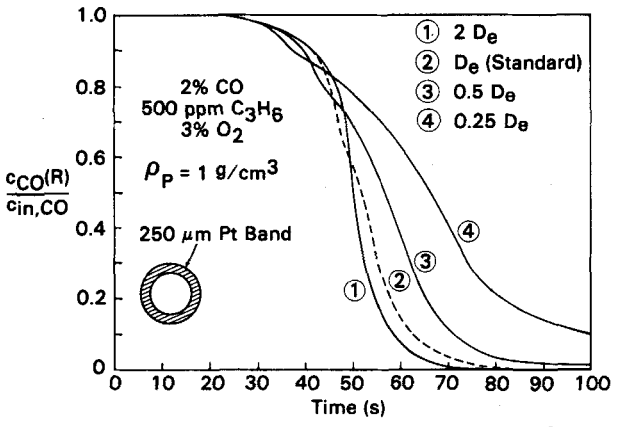

Figure 12. Effects of effective diffusivities (ρ_p fixed at 1 g/cm^3) on the lightoff behavior of a catalyst; other parameter values are listed in Table 1.

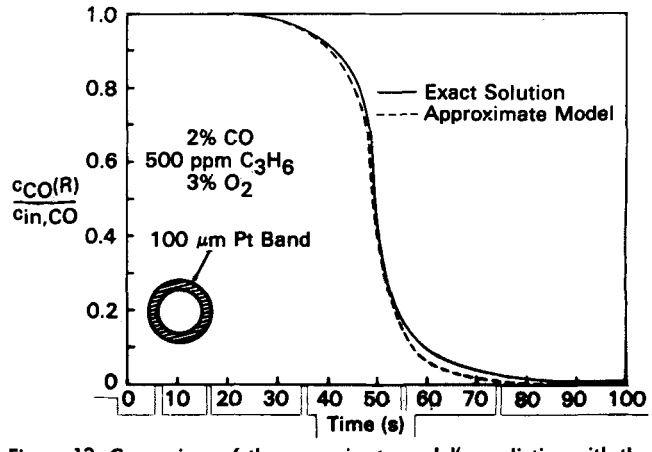

Figure 13. Comparison of the approximate model's prediction with the exact solution; parameter values are listed in Table 1.

the effective diffusivity is proportional to the void fraction of the pellet.) The product of the pellet density and Pt wt% (and thus the Pt content in one pellet) was kept constant at the standard value in these calculations.

It is of interest to investigate the effect of effective diffusivities, in view of their importance in determining the warmed-up performance. Figure 12 shows the computational results obtained when the effective diffusivities of the reactants are perturbed around their standard values listed in Table 1, while maintaining the pellet density constant at 1 g/cm^3. As might be expected, decreasing the effective diffusivity tends to improve early activity; however, when the effective diffusivity is too low, the catalyst's activity at later times is significantly sacrificed, resulting in the deterioration of the overall performance [compare curves (2) and (4)]. This detrimental effect of the sluggish lightoff, depicted by curve (4), can be minimized by increasing the effective diffusivity. Notice, however, that the performance of the catalyst becomes relatively insensitive to the variation of the effective diffusivity when it is increased beyond a certain value [compare curves (1) and (2)].

The behavior of subsurface-impregnated catalysts is similarly affected by the variation of the effective diffusivity; that is, as the effective diffusivity increases (decreases), a tradeoff again exists between improving (impairing) the steady-state performance and impairing (improving) the lightoff behavior.

It is recalled that all the computational results shown here were obtained based on a model which allows for radial temperature gradients inside the catalyst pellet. Although the assumption of uniform temperature throughout the pellet has been widely used for steady-state modeling (e.g., McGreavy and Cresswell, 1969; Smith, 1977), its validity in transient modeling has rarely been examined. Therefore, it is of interest to investigate the effect of the uniform pellet temperature approximation on the predicted transient behavior of the catalyst.

Figure 13 compares the results of the approximate model (i.e., the model with the uniform pellet temperature assumption) with the exact solution, and a good agreement is noted. [The computational results for the approximate model were obtained by assigning a sufficiently large value of λ_e (e.g., $\lambda_e = 1$) in the pellet energy balance equation so that the temperature inside the pellet is essentially uniform at all times.] This agreement provided by the approximate model can be attributed to the fact that although the temperature gradient inside the pellet is significant at early times, the intrapellet temperature profile becomes reasonably flat by the time the catalyst reaches its reaction temperatures (Figure 1). Similar agreement was also obtained for various other impregnation patterns and converter operating conditions of practical interest. The validity of the uniform pellet temperature approximation has useful implications in the simplification of a converter model; that is, it permits one to replace the energy balance on the catalyst pellet (a partial differential equation as given by Eqs. 10 to 12) by a single ordinary differential equation in the time-domain.

The single-pellet model presented here, though useful in gaining insight into catalyst lightoff, cannot be directly used to predict the actual warm-up performance of a converter, because individual pellets in the converter are exposed to different bulk gas conditions, depending on their axial location and time. For this reason, the single-pellet model has been extended to a full-converter model using a mixing cell scheme. The resulting computational results will be published later.

APPENDIX
Determination of Expansion Coefficients

The time-dependent expansion coefficients a_i^j and b^j of the Galerkin approximations (Eqs. 20 and 21) are determined by the conditions given by Eq. 22. Upon integration by parts, using the associated interface conditions and the boundary conditions, Eq. 22 becomes:

$$\int_0^R D_{e,i}(r)r^2\frac{d\hat{c}_i}{dr}\frac{dw_j}{dr}dr + \int_0^R a(r)r^2\tilde{R}_i(\hat{c},\ \hat{T})w_j(r)dr$$

$$-R^2\sigma_i[c_{\mathrm{in},i}(t) - \hat{c}_i(R,\ t)]w_j(R) = 0 \qquad (A1)$$

$$(1\le i\le 3,\ 1\le j\le M)$$

$$\int_0^R \rho_p(r)C_{ps}(r)r^2\frac{\partial\hat{T}}{\partial t}w_j(r)dr = -\int_0^R \lambda_e(r)r^2\frac{\partial\hat{T}}{\partial r}\frac{\partial w_j}{\partial r}dr + \sum_{k=1}^{2}(-\Delta H)_k\int_0^R a(r)r^2\tilde{R}_k(\hat{c},\ \hat{T})w_j(r)dr + R^2\nu[T_{\mathrm{in}}(t) - \hat{T}(R,\ t)]w_j(R) \quad (1\le i\le M) \qquad (A2)$$

where (see Eqs. 14 and 15),

$$\sigma_i = \frac{k_{m,i}}{D_{e,i}(R)(1+\alpha_i)},\quad \nu = \frac{h}{\lambda_e(R)(1+\beta)}$$

If we define the time-dependent vectors $\bar{a}_i(t)$ and $\bar{b}(t)$ by:

$$\bar{a}_i(t) \equiv [a_i^1(t),\ a_i^2(t),\ \ldots,a_i^M(t)]^T \quad (1\le i\le 3)$$

$$\bar{b}(t) \equiv [b^1(t),\ b^2(t)\ ,\ \ldots\ ,\ b^M(t)]^T,$$

then the coupled nonlinear Eqs. A1 and A2 can be expressed in terms of $\bar{a}_i(t)$ and $\bar{b}(t)$ by the matrix equations:

$$A_i\ \bar{a}_i(t) + G_i[\bar{a}_1(t),\ \bar{a}_2(t),\ \bar{a}_3(t),\ \bar{b}(t)] + \bar{s}_i(t) = 0 \qquad (A3)$$

$$(1\le i\le 3)$$

$$B\frac{d\bar{b}}{dt} = K\bar{b}(t) + F[\bar{a}_1(t),\ \bar{a}_2(t),\ \bar{a}_3(t),\ \bar{b}(t)] + \bar{v}(t) \qquad (A4)$$

where A_i, B, and K are $M\times M$ matrices with entries defined by:

$$[A_i]_{jk} = \int_0^R D_{e,i}(r)r^2\frac{dw_j}{dr}\frac{dw_k}{dr}dr + R^2\sigma_i w_j(R)w_k(R) \qquad (A5)$$

$$[B]_{jk} = \int_0^R \rho_p(r)C_{ps}(r)r^2w_j(r)w_k(r)dr \qquad (A6)$$

$$[K]_{jk} = -\int_0^R \lambda_e(r)r^2\frac{dw_j}{dr}\frac{dw_k}{dr}dr - R^2\nu w_j(R)w_k(R) \qquad (A7)$$

G_i, $\bar{s}_i$, F, and $\bar{v}$ are $M\times l$ vectors with j^{th} entry given by:

$$[G_i]_j = \int_0^R a(r)r^2\tilde{R}_i(\hat{c},\ \hat{T})w_j(r)dr \qquad (A8)$$

$$[F]_j = \sum_{i=1}^{2}(-\Delta H)_i[G_i]_j \qquad (A9)$$

$$[\bar{s}_i(t)]_j = -R^2\sigma_i c_{\mathrm{in},i}(t)w_j(R) \qquad (A10)$$

$$[\bar{v}(t)]_j = R^2\nu T_{\mathrm{in}}(t)w_j(R) \qquad (A11)$$

In Eqs. A5 to A11, the indices i, j, k range over $1\le i\le 3$, $1\le j,k\le M$.

Choice of Basis Functions

We predicate our choice of basis functions upon the desire to arrive at a well-structured algebraic/initial value problem in Eqs. A3 and A4. That is, we use basis functions $w_j(r)$ which lead to sparse band matrices A_i, B, and K in Eqs. A5 to A7. To that end, let π_M denote a partition of the interval $[0,\ R]$ into mesh points $0 = x_1 < x_2 < \ldots < x_M = R$ such that the interface points r_j (Eqs. 8 and 9) form a subset of π_M. Then, for $j=1,2,\ \ldots,\ M$, define basis functions $w_j(r)$ by:

$$w_j(r) = \begin{cases} x_j(r - x_{j-1})/rh_{j-1}, & x_{j-1}\le r\le x_j \\ x_j(x_{j+1} - r)/rh_j, & x_j\le r\le x_{j+1} \\ 0, & \text{otherwise} \end{cases} \qquad (A12)$$

where $h_j = x_{j+1} - x_j$, $1\le j\le M-1$. When $w_j(r)$ of Eq. A12 is used to derive Eqs. A3 and A4, it can be verified that A_i, B, and K of Eqs. A5 to A7 are tridiagonal matrices. Finally, since we assume that $D_{e,i}(r)$, $\rho_p(r)C_{ps}(r)$, and $\lambda_e(r)$ are piecewise constant, the entries of A_i, B, and K can be easily evaluated by exact integration. The vectors G_i and F in Eqs. A8 and A9 must be evaluated by numerical quadrature. The consistent quadrature scheme used here was based on representing the nonlinear term R_i in G_i (Eq. A8) by their interpolants in span $[w_j(r)]_{j=1}^M$ (Cavendish and Oh, 1979).

Solving the System (Eqs. A3 and A4)

Eq. A3 is a nonlinear system of algebraic equations (with time as a parameter), while Eq. A4 represents a nonlinear matrix differential

equation. These coupled equations were solved as follows. A temperature profile $\hat{T}^n(r, t)$ in Eq. 21 at a given time t^n is known. ($\hat{T}^0$ is an approximation to the initial condition given by Eq. 13.) This (piecewise rational) temperature profile is used in Eq. A3 to find the corresponding concentration profiles in the catalyst. Using these concentration profiles, Eq. A4 is then integrated through a single time step to find the temperature $\hat{T}^{n+1}(r, t)$ at the next time level t^{n+1}. To accomplish the time integration, the GEARIB (Hindmarsh, 1976) Fortran subroutine code was used. The basic methods used in GEARIB are of the implicit linear multistep type. High numerical accuracy is achieved at minimal computer cost by permitting both the time step and the order of the multistep method to vary in a dynamic way throughout the time evolution of the problem. Time steps were controlled such that concentration profiles at consecutive time steps differed by no more than 3%. Pellet concentrations at a given time level were determined by solving Eq. A3 using Newton's method. Finally, initial guesses for Newton's method were provided by the concentration profiles found from the previous time step.

NOTATION

a = local platinum surface area (cm^2 Pt/cm^3 pellet)
c_i = concentration of species i in the catalyst pellet (mol/cm^3)
$\bar{c}$ = vector whose entries are species concentrations
$c_{\infty,i}$ = concentration of species i in the bulk gas phase surrounding the catalyst pellet (mol/cm^3)
$c_{\text{in},i}$ = concentration of species i in the incoming gas stream (mol/cm^3)
C_{pg} = heat capacity of gas (J/g · K)
C_{ps} = heat capacity of catalyst pellet (J/g · K)
$D_{e,i}$ = effective diffusivity of species i in the catalyst pellet (cm^2/s)
h = heat transfer coefficient (J/cm^2 · s · K)
$(-\Delta H)_i$ = heat of combustion of species i (J/mol)
k_i = rate constant for reaction i (cm^4/s · mol)
$k_{m,i}$ = mass transfer coefficient of species i (cm/s)
K_i = adsorption equilibrium constant for species i (cm^3/mol)
P = pressure (kPa)
Q = gas volumetric flow rate (cm^3/s)
r = pellet radial coordinate (cm)
r_j = radial location of the zone boundary in the catalyst pellet (cm)
R = radius of a spherical catalyst pellet (cm)
R_i = specific reaction rate for species i (mol/cm^2 Pt · s)
t = time (s)
T = temperature in the catalyst pellet (K)
T^0 = initial temperature in the catalyst pellet (K)
T_∞ = temperature of the bulk gas phase surrounding the catalyst pellet (K)
T_{in} = temperature of the incoming gas stream (K)
V_{cell} = volume of a mixing cell (cm^3)

Greek Letters

α_i = dimensionless quantity defined by Eq. 16
β = dimensionless quantity defined by Eq. 17
ϵ = bed void fraction
ϵ_p = pellet void fraction
ρ_g = gas density (g/cm^3)
ρ_p = pellet density (g/cm^3)
λ_e = effective thermal conductivity in the catalyst pellet (J/cm · s · K)

LITERATURE CITED

Bauerle, G. L., and K. Nobe, "Two-Stage Catalytic Converter: Transient Operation," *Ind. Eng. Chem. Proc. Design Develop.*, **12**, 407 (1973).

Becker, E. R., and J. Wei, "Catalyst Design for Reactions of Negative Order," *Proceedings of the 4th Int. Symp. Chem. Reaction Eng.*, Heidelberg, W. Germany, VII-300 (April, 1976).

Becker, E. R., and J. Wei, "Nonuniform Distribution of Catalysts on Supports I. Bimolecular Langmuir Reactions," *J. Catal.*, **46**, 365 (1977a).

Becker, E. R., and J. Wei, "Nonuniform Distribution of Catalysts on Supports II. First Order Reactions with Poisoning," *J. Catal.*, **46**, 372 (1977b).

Bird, R. B., W. E. Stewart, and E. N. Lightfoot, *Transport Phenomena*, John Wiley, New York (1960).

Cavendish, J. C., and S. H. Oh, "A Computationally Efficient Galerkin Technique for Approximating Transient Diffusion-Reaction Equations in Composite Media," *Chem. Eng. J.*, **17**, 41 (1979).

De Acetis, J., and G. Thodos, "Flow of Gases Through Spherical Packings," *Ind. Eng. Chem.*, **52**, 1003 (1960).

Ferguson, N. B., and B. A. Finlayson, "Transient Modeling of a Catalytic Converter to Reduce Nitric Oxide in Automobile Exhaust," *AIChE J.*, **20**, 539 (1974).

Finlayson, B. A., *The Method of Weighted Residuals and Variational Principles*, Academic Press, New York (1972).

Harned, J. L., "Analytical Evaluation of a Catalytic Converter System," SAE Paper 720520 (1972).

Hegedus, L. L., and J. C. Summers, "Improving Automotive Catalysts' Tolerance to Poisoning," *4th North American Meeting of The Catalysis Soc.*, Toronto, Canada, February 1975.

Hegedus, L. L., and J. C. Cavendish, "Intrapellet Diffusivities from Integral Reactor Models and Experiments," *Ind. Eng. Chem. Fundam.*, **16**, 356 (1977).

Hegedus, L. L., S. H. Oh, and K. Baron, "Multiple Steady States in an Isothermal, Integral Reactor: The Catalytic Oxidation of Carbon Monoxide Over Platinum-Alumina," *AIChE J.*, **23**, 632 (1977).

Hegedus, L. L., and J. C. Summers, "Improving the Poison Resistance of Supported Catalysts," *J. Catal.*, **48**, 345 (1977).

Hegedus, L. L., J. C. Summers, J. C. Schlatter, and K. Baron, "Poison-Resistant Catalysts for the Simultaneous Control of Hydrocarbon, Carbon Monoxide, and Nitrogen Oxide Emissions," *J. Catal.*, **56**, 321 (1979).

Herod, D. M., M. V. Nelson, and W. M. Wang, "An Engine Dynamometer System for the Measurement of Converter Performance," SAE Paper 730557 (1973).

Hindmarsh, A. C., "GEARIB, Solution of Implicit Systems of Ordinary Differential Equations with Banded Jacobian," Lawrence Livermore Laboratory Report UCID 30130 (February, 1976).

Kuo, J. C. W., C. R. Morgan, and H. G. Lassen, "Mathematical Modeling of CO and HC Catalytic Converter Systems," SAE Paper 710289 (1971).

McGreavy, C., and D. L. Cresswell, "A Lumped Parameter Approximation to a General Model for Catalytic Reactors," *Can. J. Chem. Eng.*, **47**, 583 (1969).

Oh, S. H., K. Baron, J. C. Cavendish, and L. L. Hegedus, "Carbon Monoxide Oxidation in an Integral Reactor: Transient Response to Concentration Pulses in the Regime of Isothermal Multiplicities," *ACS Symposium Ser.*, **65**, 461 (1978).

Schlatter, J. C., Private communications, General Motors Research Laboratories, Warren, Mich. (1976).

Smith, J. M., *Chemical Engineering Kinetics*, McGraw-Hill, New York (1970).

Smith, T. G., "An Examination of the Isothermal Pellet Assumption Relative to the Design of Nonadiabatic Fixed Bed Catalytic Reactors," *Chem. Eng. Sci.*, **32**, 1023 (1977).

Summers, J. C., and L. L. Hegedus, "Effects of Platinum and Palladium Impregnation on the Performance and Durability of Automobile Exhaust Oxidizing Catalysts," *J. Catal.*, **51**, 185 (1978).

Voltz, S. E., C. R. Morgan, D. Liederman, and S. M. Jacob, "Kinetic Study of Carbon Monoxide and Propylene Oxidation on Platinum Catalysts," *Ind. Eng. Chem. Prod. Res. Develop.*, **12**, 294 (1973).

Wei, J., "Catalysis for Motor Vehicle Emissions," *Advan. Catal.*, **24**, 57 (1975).

Young, L. C., and B. A. Finlayson, "Mathematical Models of the Monolith Catalytic Converter: Part II. Application of Automobile Exhaust," *AIChE J.*, **22**, 343 (1976).

Manuscript received August 8, 1979; revision received March 20, and accepted April 10, 1980.